

**Oxygen defect and Si nanocrystal dependent white-light and near-infrared electroluminescence of Si-implanted and plasma-enhanced chemical-vapor deposition-grown Si-rich SiO<sub>2</sub>**

Gong-Ru Lin, Chun-Jung Lin, Chi-Kuan Lin, Li-Jen Chou, and Yu-Lun Chueh

Citation: *Journal of Applied Physics* **97**, 094306 (2005); doi: 10.1063/1.1886274

View online: <http://dx.doi.org/10.1063/1.1886274>

View Table of Contents: <http://scitation.aip.org/content/aip/journal/jap/97/9?ver=pdfcov>

Published by the [AIP Publishing](#)

---

**Articles you may be interested in**

[N<sub>2</sub>O-grown oxides/4H-SiC\(0001\), \(003 \$\bar{3}\$ 8\), and \(112 \$\bar{0}\$ \) interface properties characterized by using p-type gate-controlled diodes](#)

*Appl. Phys. Lett.* **93**, 193510 (2008); 10.1063/1.3028016

[Oxide scalability in Al<sub>2</sub>O<sub>3</sub>/Ga<sub>2</sub>O<sub>3</sub>\(Gd<sub>2</sub>O<sub>3</sub>\)In<sub>0.20</sub>Ga<sub>0.80</sub>As/GaAs heterostructures](#)

*J. Vac. Sci. Technol. B* **26**, 1132 (2008); 10.1116/1.2884739

[Fourfold increase of the ultraviolet \(314 nm\) electroluminescence from SiO<sub>2</sub>:Gd layers by fluorine coimplantation and flash lamp annealing](#)

*Appl. Phys. Lett.* **91**, 181107 (2007); 10.1063/1.2803855

[Electrical characterization of SiO<sub>2</sub>/n-GaN metal-insulator-semiconductor diodes](#)

*J. Vac. Sci. Technol. B* **21**, 1364 (2003); 10.1116/1.1591740

[Charge centers induced in thermal SiO<sub>2</sub> films by high electric field stress at 80 K](#)

*J. Appl. Phys.* **89**, 3337 (2001); 10.1063/1.1350414

---



## Re-register for Table of Content Alerts

Create a profile.



Sign up today!



# Oxygen defect and Si nanocrystal dependent white-light and near-infrared electroluminescence of Si-implanted and plasma-enhanced chemical-vapor deposition-grown Si-rich SiO<sub>2</sub>

Gong-Ru Lin,<sup>a)</sup> Chun-Jung Lin, and Chi-Kuan Lin

Department of Photonics and Institute of Electro-Optical Engineering, National Chiao Tung University, 1001 Ta Hsueh Road, Hsinchu, Taiwan 300, Republic of China

Li-Jen Chou and Yu-Lun Chueh

Department of Materials Science and Engineering, National Tsing Hua University, 101, Section 2 Kuang Fu Road, Hsinchu, Taiwan 300, Republic of China

(Received 29 July 2004; accepted 15 February 2005; published online 20 April 2005)

The mechanisms for silicon (Si) defect and nanocrystal related white and near-infrared electroluminescences (ELs) of Si-rich SiO<sub>2</sub> films synthesized by Si-ion implantation and plasma-enhanced chemical-vapor deposition (PECVD) are investigated. The strong photoluminescence (PL) of Si-ion-implanted SiO<sub>2</sub> (SiO<sub>2</sub>:Si<sup>+</sup>) at 415–455 nm contributed by weak-oxygen bond and neutral oxygen vacancy defects is observed after 1100 °C annealing for 180 min. The white-light EL of a reverse-biased SiO<sub>2</sub>:Si<sup>+</sup> metal-oxide-semiconductor (MOS) diode with a turn-on voltage of 3.3 V originates from the minority-carrier tunneling and recombination in the defect states of SiO<sub>2</sub>:Si<sup>+</sup>, which exhibits maximum EL power of 120 nW at bias of 15 V with a power-current slope of 2.2 μW/A. The precipitation of nanocrystallite silicon (nc-Si) in SiO<sub>2</sub>:Si<sup>+</sup> is less pronounced due to relatively small excess Si density. In contrast, the 4-nm nc-Si contributed to PL and EL at about 760 nm is precipitated in the PECVD-grown Si-rich SiO<sub>x</sub> film after annealing at 1100 °C for 30 min. The indium-tin-oxide/Si-rich SiO<sub>x</sub>/p-Si/Al metal oxide semiconductor (MOS) diode is highly resistive with turn-on voltage and power-current (*P*–*I*) slope of 86 V and 0.7 mW/A, respectively. The decomposed EL peaks at 625 and 768 nm are contributed by the bias-dependent cold-carrier tunneling between the excited states in adjacent nc-Si quantum dots.

© 2005 American Institute of Physics. [DOI: 10.1063/1.1886274]

## I. INTRODUCTION

Versatile technologies have been proposed for fabricating nanocrystallite silicon (nc-Si) structures, such as electron-beam evaporation,<sup>1</sup> rf-magnetron sputtering, Si-ion implantation,<sup>2</sup> and plasma-enhanced chemical-vapor deposition<sup>3</sup> (PECVD). Most nc-Si-based materials have been shown to exhibit strong photoluminescence (PL) and visible electroluminescence (EL) at room temperature, in which the blue-green emission is of great interest. The room-temperature PL of porous Si,<sup>4</sup> Si-rich SiO<sub>2</sub> grown by PECVD, and Si-ion-implanted SiO<sub>2</sub> (SiO<sub>2</sub>:Si<sup>+</sup>) has stimulated comprehensive studies on light-emitting devices made from nc-Si structures. The nc-Si structures formed by different processing methods yield different PL peaks in the blue-green band (415, 437, 470, and 490–540 nm),<sup>5–7</sup> the orange-red band (570, 600, 630, and 645 nm),<sup>1,6,7</sup> and the near infrared region (710–800 nm).<sup>8</sup> In particular, a strong PL at 340–370 nm from as-grown *a*-Si:H:O films<sup>9</sup> deposited by PECVD at low substrate temperatures has also been reported. Recently, the identification of categories of defects in Si-implanted SiO<sub>2</sub> films with a stable blue emission at 400–500 nm has attracted great interest.<sup>10</sup> Silicon implantation introduces several types of point defects in SiO<sub>2</sub>,<sup>11</sup> such as

the *E'* center [O<sub>3</sub>≡Si•], the neutral oxygen vacancy (NOV) [O<sub>3</sub>≡Si–Si≡O<sub>3</sub>], the nonbridging oxygen hole center (NBOHC) [O<sub>3</sub>≡Si–O•], the peroxy radical [O<sub>3</sub>≡Si–O–O•],<sup>12</sup> the *D* center [(Si<sub>3</sub>≡Si•)<sub>n</sub>],<sup>6,13</sup> and other interstitial defects. The densities of these defects in the as-implanted SiO<sub>2</sub>:Si<sup>+</sup> samples are changed, normally reduced, at various rates during thermal annealing. Some of these defects, such as NOV and NBOHC, are the principal radiative recombination centers or the so-called luminescence centers. Hayes *et al.*<sup>14</sup> found that a transient pair of an oxygen vacancy and oxygen interstice contributes to the 2.7-eV PL. Nishikawa *et al.*<sup>15</sup> and Tohmon *et al.*<sup>16</sup> attributed the origin of the PL peak at 470 nm to the NOV defect. These Si–O related species have previously been identified as the defects in SiO<sub>2</sub>:Si<sup>+</sup> that dominate the blue-green light emission, while the nc-Si embedded in the SiO<sub>2</sub> matrix contributes to the emission at longer wavelengths, due to quantum confinement.<sup>11</sup> That is, the SiO<sub>2</sub>:Si<sup>+</sup> material may concurrently exhibit two contradictory mechanisms with different emission ranges, which leads to different luminescent result as compared to the PECVD-grown Si-rich SiO<sub>x</sub> (*x*<2) material with similar annealing conditions. Linnros and co-workers<sup>17,18</sup> have analyzed the nearly coincident PL and EL spectra of the *n*<sup>+</sup>-Si/SiO<sub>x</sub>/p<sup>+</sup>-Si metal-oxide-semiconductor (MOS) diode with nc-Si embedding in the SiO<sub>x</sub> matrix. Iacona *et al.* further demonstrated the control on the nc-Si size by varying the SiO<sub>x</sub> stoichiometry or annealing

<sup>a)</sup>Author to whom correspondence should be addressed; FAX: +886-3-5716631; electronic mail: grlin@faculty.nctu.edu.tw

temperature,<sup>19</sup> giving rise to the shift in central PL wavelength from 700 to 900 nm. Franzo *et al.*<sup>20</sup> confirmed that the PL and EL of the PECVD-grown Si-rich SiO<sub>x</sub> film exhibit same luminescent mechanism, which result from the *e-h* recombination within the nc-Si. In addition, the observation of a small defect-related EL peak at 660 nm was also addressed. However, the comparisons and interpretations on the defect- and nc-Si-dependent current–voltage responses, PL and EL properties, and corresponding mechanisms of the Si-implanted SiO<sub>2</sub> and PECVD-grown Si-rich SiO<sub>x</sub> were seldom addressed before. In this work, the experimental evidences and corresponding mechanisms of the defect- or nc-Si-related PL and EL from two MOS diodes fabricated on Si-implanted SiO<sub>2</sub>:Si<sup>+</sup>/Si and PECVD-grown Si-rich SiO<sub>x</sub>/Si substrates are investigated, compared, and elucidated in more detail.

## II. EXPERIMENT

The SiO<sub>2</sub>:Si<sup>+</sup> samples were prepared by multienergy Si-implantation of the 5000-Å-thick SiO<sub>2</sub> film grown on the *n*-type (100)-oriented Si substrate with a resistivity of 4–7 Ω cm. The SiO<sub>2</sub> film was deposited by PECVD at chamber pressure of 400 mTorr using 10-SCCM (standard cubic centimeter per minute) tetraethoxysilane (TEOS) fluence and 200-SCCM O<sub>2</sub> fluence at a forward power of 150 W. The recipes of the multienergy Si implantation are 5 × 10<sup>15</sup> ions/cm<sup>2</sup> at 40 keV, 1 × 10<sup>16</sup> ions/cm<sup>2</sup> at 80 keV, and 2 × 10<sup>16</sup> ions/cm<sup>2</sup> at 150 keV. On the other hand, the Si-rich SiO<sub>x</sub> film was grown on a *p*-type (100)-oriented Si substrate by using a PECVD system at pressure of 70 mTorr and a N<sub>2</sub>O/SiH<sub>4</sub> fluence ratio of 6:1 under a forward power of 60 W. The N<sub>2</sub>O fluence was controlled at 120 SCCM. The excess Si atom density is calculated by using a Monte Carlo simulating program “transport of ions in matter (TRIM) code,” which shows a nearly flat-topped implantation profile at depths between 100 and 5000 Å below the sample surface. In addition, the secondary-ion-mass spectrometry (SIMS) of excess Si profile in the SiO<sub>2</sub>:Si<sup>+</sup> and Si-rich SiO<sub>x</sub> samples is also performed, showing good agreement with the TRIM results. Afterwards, the SiO<sub>2</sub>:Si<sup>+</sup> and Si-rich SiO<sub>x</sub> films were postannealed in quartz furnace with flowing N<sub>2</sub> gas at 1100 °C for 30–240 min, which helps to activate the radiative defects or to precipitate the nc-Si in these samples. To characterize the EL response, the samples were diced to 1 × 1 mm<sup>2</sup> and were evaporated with Ag (on the top of SiO<sub>2</sub>:Si<sup>+</sup>) or indium-tin-oxide (ITO) (on the top of Si-rich SiO<sub>x</sub>) to form the MOS diodes. The contact thickness and diameters were set as 2000 Å and 0.8 mm, respectively. A 5000-Å Al contact electrode was coated on the bottom of the Si substrate.

After annealing, the room-temperature continuous-wave (cw) PL was performed using a He–Cd laser with a wavelength and average intensity of 325 nm and 5 W/cm<sup>2</sup>, respectively. The PL range from 360 to 900 nm was resolved by a fluorescent spectrophotometer (Jobin Yvon, TRIAX-320) using a 1200-g/mm grating with a wavelength resolution of 0.06 nm, and detected by a cooled photomultiplier (Jobin Yvon, Model 1424M) -based photon counter. The

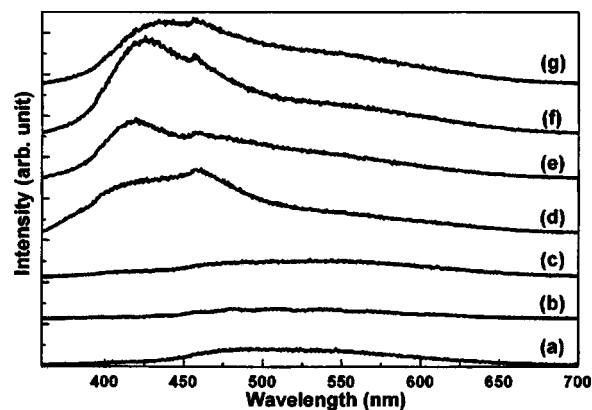


FIG. 1. PL spectra of the (a) *n*-type Si substrate, (b) SiO<sub>2</sub>/*n*-Si sample, and the SiO<sub>2</sub>:Si<sup>+</sup>/Si samples in (c) as-implanted condition, or annealed at 1100 °C for (d) 30 min, (e) 60 min, (f) 180 min, and (g) 240 min.

working distance between the focusing lens and the sample was fine-tuned to maximize the PL intensity. The EL ranged from 300 to 1100 nm was detected by a charge-coupled device (CCD)-based spectrum (Ocean Optics, USB-2000). The MOS diode was driven by either a programmable electrometer (Keithley, model 6517) with resolution as low as 100 fA or a voltage source meter (Keithley, 236), which uses micro-probes (Karr Suss, 253). The optical power was measured using an optical multimeter (ILX, 6810B). An integrated sphere detector (ILX, OMH-6703B) was employed to collect the light emitted from the surface of the SiO<sub>2</sub>:Si<sup>+</sup> MOS diode.

## III. PHOTOLUMINESCENCE AND CORRESPONDING MECHANISMS

### A. PL of Si-implanted SiO<sub>2</sub>

The PL spectra of the Si substrate [Fig. 1, line (a)], unimplanted [Fig. 1, line (b)], and implanted [Fig. 1, line (c)] SiO<sub>2</sub>:Si<sup>+</sup> on Si samples without annealing are shown in Fig. 1. The Si or unimplanted SiO<sub>2</sub>/Si substrate presents a weak and broad PL spectrum between 400 and 600 nm, which becomes much weaker after annealing at 1100 °C for 60 min. In contrast, the Si-ion implantation introduces enormous radiative defects into the SiO<sub>2</sub> film, which causes a strong PL peak at around 410–460 nm for the SiO<sub>2</sub>:Si<sup>+</sup> sample, after annealing at 1100 °C for 30 min, as shown in Fig. 1. Previously, the luminescent centers in the SiO<sub>2</sub>:Si<sup>+</sup> corresponding to the visible PL were comprehensively investigated, which include the B<sub>2</sub> center,<sup>21</sup> the weak-oxygen bond (WOB),<sup>22</sup> the NOV defect,<sup>5,15,16</sup> the E'<sub>δ</sub> defect,<sup>15</sup> and the NBOHC defects<sup>9–11</sup> at emitting wavelengths of around 281, 415, 455, 520, and 630 nm, respectively. According to the PL spectrum shown in Fig. 1, it is obvious that there are at least two PL peaks at 400–600-nm region, which is enhanced after furnace annealing at 1100 °C for 180 min. After decomposing with multi-Gaussian function, three principle luminescent centers at 415, 455, and 520 nm with spectra linewidths of 35, 52, and 150 nm, respectively, are demonstrated.<sup>1,8,12,13</sup> The strongest PL peaks at 415–455 nm with linewidths of 35–50 nm are very similar to those obtained by Cheang-Wong *et al.*<sup>22</sup> and Nishikawa *et al.*<sup>23</sup> The luminescence at

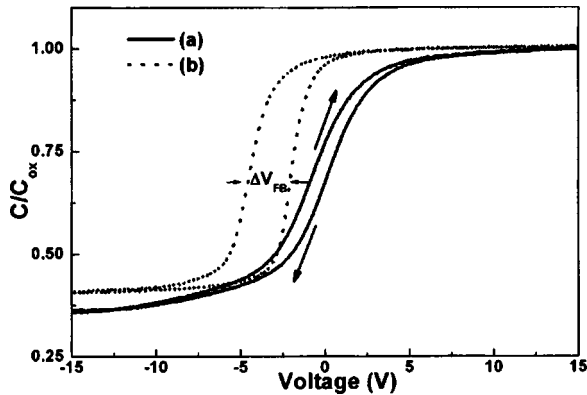


FIG. 2.  $C$ - $V$  hysteresis measurement of the MOS diode made on (a) as-implanted  $\text{SiO}_2:\text{Si}^+$  and (b)  $\text{SiO}_2:\text{Si}^+$  annealed at  $1100\text{ }^\circ\text{C}$  for 180 min.

455 nm reported by Bae *et al.*<sup>24</sup> has been attributed to the transition between the ground state (singlet) and the elevated state (triplet)<sup>25,26</sup> of the NOV defect.

In principle, the NOV defects ( $\text{O}_3 \equiv \text{Si}-\text{Si} \equiv \text{O}_3$ ) are created by the displacement of oxygen from a normal  $\text{SiO}_2$  structure during the Si implantation,<sup>15</sup> and the oxygen interstitials are concurrently generated under the physical destruction process. This process can be described by the reaction rule of  $\text{O}_3 \equiv \text{Si}-\text{O}-\text{Si} \equiv \text{O}_3 \rightarrow \text{O}_3 \equiv \text{Si}-\text{Si} \equiv \text{O}_3 + \text{O}_{\text{interstitial}}$ .<sup>16,22,24</sup> Liao *et al.* have observed a stable blue emission ( $\sim 2.7$ -eV band),<sup>10</sup> attributed to the NOV defect, from the Si-ion-implanted  $\text{SiO}_2$  films thermally grown on the Si substrate under ultraviolet excitation. Such a 2.7-eV PL can also be found in bulk  $\text{SiO}_2$  or high-purity silica glass exhibit at low temperatures.<sup>16,24,25</sup> Si-implanted thermal  $\text{SiO}_2$ ,<sup>16</sup> Ge-implanted  $\text{SiO}_2$ ,<sup>24</sup>  $\text{Ir}^{2+}$ -implanted silica glass,<sup>22</sup> etc. The diamagnetic NOV defect is the precursor to the formation of the paramagnetic  $E'$  center ( $\text{O}_3 \equiv \text{Si}^+\text{Si} \equiv \text{O}_3$ ), which is formed by trapping a hole at the site of the NOV (a positively charged oxygen vacancy).<sup>25</sup> That is,  $\text{O}_3 \equiv \text{Si}-\text{Si} \equiv \text{O}_3 + h^+ \rightarrow \text{O}_3 \equiv \text{Si}^+\text{Si} \equiv \text{O}_3$ , where  $h^+$  denotes the trapped hole state. Hole trapping yields a positively charged NOV defect ( $\text{O}_3 \equiv \text{Si}^+\text{Si} \equiv \text{O}_3$ ) or the so-called  $E'$  center in  $\text{SiO}_2:\text{Si}^+$ , which can induce a space-charge effect and inevitably leads to the clear hysteresis in the capacitance-voltage ( $C$ - $V$ ) response of a MOS diode made on  $\text{SiO}_2:\text{Si}^+$ . According to the high-frequency  $C$ - $V$  curves for as-implanted and 180-min-annealed  $\text{SiO}_2:\text{Si}^+$  metal-oxide-semiconductor diodes (see Fig. 2), the hysteresis is attributed to the trapping of hole (or electron) in the insulator during the positive (or negative) gate voltage sweeping. The concentration of the NOV defects can be determined from the flatband voltage shift of the  $C$ - $V$  hysteresis. The density of hole trapped NOV defects in  $\text{SiO}_2:\text{Si}^+$  ( $N_{\text{NOV}}$ ) is obtained from the equation of  $N_{\text{NOV}} = -\Delta V_{\text{FB}} C_{\text{ox}} / e$ , where  $C_{\text{ox}}$  is the capacitance of the  $\text{SiO}_2:\text{Si}^+$  in strong accumulation regime and  $\Delta V_{\text{FB}}$  is the flatband voltage shift. For example, the as-implanted  $\text{SiO}_2:\text{Si}^+$  exhibits a flatband voltage shift ( $\Delta V_{\text{FB}}$ ) of  $-0.89\text{ V}$  corresponding to a NOV defect concentration of  $8 \times 10^{16}\text{ cm}^{-3}$ . Therefore, the existence of the NOV defect with PL at the wavelength of 455 nm is confirmed.

Since the oxygen interstitials are concurrently generated with the NOV defects during the Si implantation, the WOB

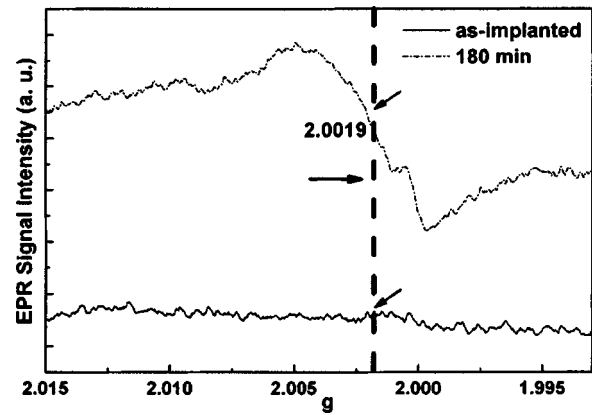


FIG. 3. EPR spectrum of the as-grown and 180-min-annealed  $\text{SiO}_2:\text{Si}^+$ .

defects can be formed and activated after thermal annealing by the reaction rule of  $\text{O}_{\text{interstitial}} + \text{O}_{\text{interstitial}} \rightarrow \text{O}-\text{O}$ . Nishikawa *et al.* have primarily discussed that the WOB defect is the precursor of the NBOHC defect,<sup>27</sup> which is also a pre-existing defect in silica responsible for the 3.1-eV PL under the pumping of such paramagnetic centers by 6.4-eV photons. The origin for the cwPL at 520 nm was previously identified as the emission of the  $E'_\delta$  defect (a paramagnetic state of Si cluster or a delocalized variant of the  $E'$  center) by Chou *et al.*<sup>28</sup> They concluded that a deficiency of oxygen and hydrogenous species could create the  $E'_\delta$  defect in  $\text{SiO}_2:\text{Si}^+$  films after rapid thermal annealing at  $\geq 950\text{ }^\circ\text{C}$ . Nishikawa *et al.*<sup>29</sup> also reported that the intensity of the 2.2-eV band in oxygen-deficient-type amorphous  $\text{SiO}_2$  ( $\alpha\text{-SiO}_2$ ) is correlated with the concentration of the  $E'_\delta$  center. Some observations also suggest that the  $E'_\delta$  defect is based on the existence of small amorphous Si cluster<sup>6,8</sup> or its precursor<sup>4</sup> in  $\text{SiO}_2:\text{Si}^+$  or  $\text{Si}:\text{O}^+$  materials. The  $E'_\delta$  center is generally an unpaired spin delocalized over five Si atoms, which can be examined by the electron-spin-resonance (EPR) measurement. Figure 3 shows the EPR spectra for the  $\text{SiO}_2:\text{Si}^+$  samples before and after annealing. No significant EPR feature can be observed in the as-implanted  $\text{SiO}_2:\text{Si}^+$ . After annealing, a gradually enlarged EPR signal with zero crossing  $g$  value of 2.0019 is attributed to the formatted  $E'_\delta$  defect (generally depicted as  $\text{Si} \uparrow \text{Si} \equiv \text{Si}$ ).<sup>29,30</sup> The EPR intensity increases by two times as the annealing time more lengthens to 180 min, which is relatively in good agreement with the cwPL analysis.<sup>31,32</sup>

Figure 4 plots the evolution of the peak wavelength and the associated intensity, respectively, as functions of the annealing time. The PL results indicate that the optimized annealing time for stabilizing the PL wavelength is 180 min (at  $1100\text{ }^\circ\text{C}$ ). The activation of the radiative defects is accelerated during the first 15 min, while the NOV defect becomes more pronounced than that of the WOB defects. This inevitably leads to a slight redshift of the PL from 415 to 455 nm. After annealing for 180 min or longer, the PL intensities at 415 and 455 nm decline considerably, whereas the PL intensity at 520 nm tends to remain or slightly grows. It is thus concluded that the dominant radiative defects have changed from Si-O species (i.e., WOB and NOV defects) to the  $E'_\delta$  or NBOHC defects. Note that the PL spectra of the annealed

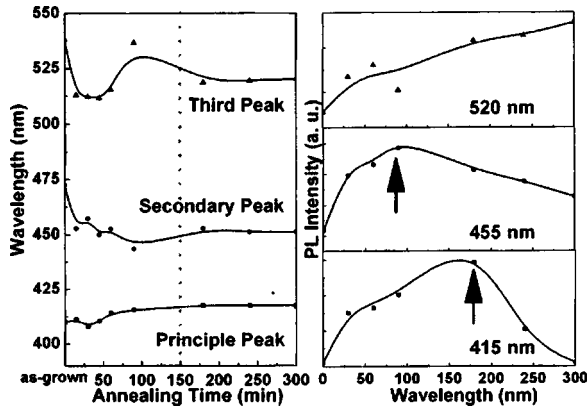


FIG. 4. Left: central wavelength of the three principal PL peaks in  $\text{SiO}_2:\text{Si}^+$  as implanted or annealed at  $1100^\circ\text{C}$  for different annealing time. Right: annealing-time-dependent PL intensities at different wavelengths of 415, 455, and 520 nm.

$\text{SiO}_2:\text{Si}^+$  samples only show very weak nc-Si-dependent fluorescence at the wavelength range from 700 to 900 nm, which reveals the extremely low density of the nc-Si embedded in the  $\text{SiO}_2$ . This result follows from the low-dose implantation process, which yields a low Si excess density of  $<3\%$  in the  $\text{SiO}_2$  matrices. In this case, insufficient nc-Si precursors are formed during the annealing process. Hence, it is not contradictory that only the blue-green emission (without any distinct sign of red or infrared emission) is observed from the  $\text{SiO}_2:\text{Si}^+$  samples.

### B. PL of PECVD-grown Si-rich $\text{SiO}_x$

The PL spectra of the PECVD-grown Si-rich  $\text{SiO}_x$  at different annealing conditions are shown in Fig. 5. The as-grown sample shows a small but broadband PL signal at 400–650 nm due to the structural defects, whereas the PL signal between 700 and 800 nm is too weak to be found. It was found that the PL is attributed to the radiative defects including the NOV (Ref. 24) and the NBOHC (Ref. 33) in the as-grown  $\text{SiO}_x$  sample. However, the defect-related PL is eliminated and the near-infrared PL intensity is greatly enhanced after annealing at  $1100^\circ\text{C}$  for 15 min, which exhibits a central wavelength of 735 nm and a spectral linewidth of about 130 nm. Such a variation in the wavelength only oc-

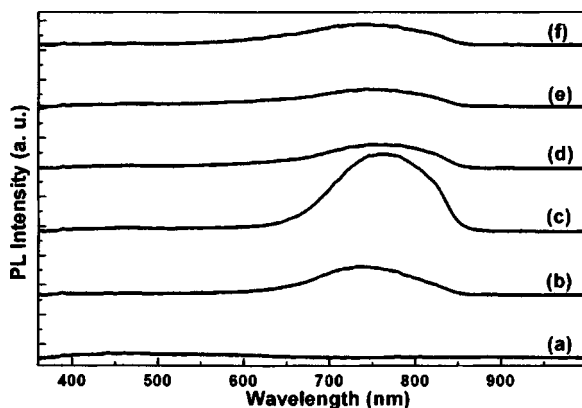


FIG. 5. PL spectra of the PECVD-grown Si-rich  $\text{SiO}_x$  in (a) as-grown condition, or annealed at  $1100^\circ\text{C}$  for (b) 15 min, (c) 30 min, (d) 60 min, (e) 120 min, and (f) 180 min.

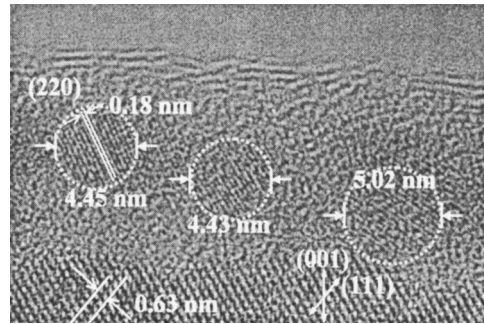


FIG. 6. High-resolution TEM of the 30-min-annealed PECVD-grown Si-rich  $\text{SiO}_x$  sample.

cur when the precipitating process of nc-Si is initiating. The growth of nc-Si becomes very fast as the excess Si atoms in the  $\text{SiO}_x$  film experience sufficient energy. In Fig. 6, the bright-field cross-sectional viewing photograph of cross-sectional high-resolution transmission electron microscopy (HRTEM) supports the existence of nc-Si with diameters of 4–5 nm in the Si-rich  $\text{SiO}_x$  sample annealed at  $1100^\circ\text{C}$  for 30 min. By employing the lattice distance of 0.63 nm between two (111)-oriented planes of the Si substrate as a standard ruler, the smaller plane-to-plane distance of (220)-oriented nc-Si of about 0.19 nm is observed. The observed nc-Si size correlates well the theoretical value of  $\lambda = 1.24/(1.12 + 3.73/d^{1.39})$  as reported by Delerue *et al.*<sup>34</sup> As the annealing time lengthens to 30 min, the strongest PL intensity is redshifted to 760 nm with the remaining linewidth. The redshift in PL between the 30-min and 15-min-annealed sample is about 26 nm. Figure 5 shows that the formation and the size increase of nc-Si are pronounced during the first 30 min. Nonetheless, a longer annealing time decreases half the PL intensity and makes the PL signal slightly blueshifted and broadened. During long-term annealing, the nc-Si reduces its size since the oxygen atoms invade the silicon atoms to construct  $\text{SiO}_2$ . After annealing for 120 min or longer, the PL of the Si-rich  $\text{SiO}_x$  becomes even smaller and broader than that annealed for 15 min.

The reoxidation problem of the nc-Si buried in the  $\text{SiO}_x$  matrix is considered since the PL is blueshifted and attenuated due to the decrease in size and density of the nc-Si. This has been confirmed by transmission electron microscopy (TEM) analysis of the annealing-time-dependent nc-Si size in the Si-rich  $\text{SiO}_x$  (see Fig. 6), which clearly indicates a decreasing trend in both the diameter and surface density as a function of the annealing time. According to the equation  $I \propto \sigma \phi(t)(1/\tau_R)N$ , the intensity of PL is proportional to the pumping flux, the cross-section area, and density of nanocrystallite Si, and is inversely proportional to the lifetime of nc-Si. This means that the density of nc-Si can abruptly decrease with either the PL intensity or the lifetime of the nc-Si if the absorption cross-section area of nc-Si and the pumping flux is kept constant. A time-resolved PL analysis reveals that the lifetime of the nc-Si is decreased from 52 to 20  $\mu\text{s}$  for the samples annealed from 30 to 120 min. Furthermore, the TEM estimated densities of nc-Si also show a decreasing trend as the annealing time lengthens. On the other hand, Iacona *et al.* reported another possible mechanism corre-

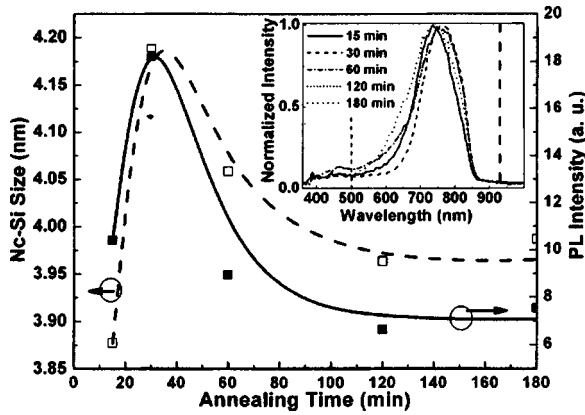


FIG. 7. Annealing-time-dependent PL intensity (solid) and size (dashed) of nc-Si. Inset: the normalized PL intensity for the annealed PECVD-grown Si-rich  $\text{SiO}_x$  samples.

sponding to the abrupt decrease of the nc-Si-related PL intensity, which states that the peak PL wavelength is mainly determined by the large nc-Si since the luminescence from the smaller nc-Si can be reabsorbed by the larger one.<sup>19</sup> Although the density of the nc-Si with size ranging between 0.7 and 2.1 nm is increased, there are only longer PL tails in the shorter-wavelength region. In this case, a sharp PL shape in the longer-wavelength region of the PL spectra is obtained, which correlates well with our experimental observations shown in the inset of Fig. 7. The broadened and blueshifted PL signal strongly supports the reoxidation effect of nc-Si in the long-term-annealed samples.

#### IV. ELECTROLUMINESCENCE AND CORRESPONDING MECHANISMS

##### A. EL and $I$ - $V$ of $\text{SiO}_2:\text{Si}^+$ -based MOS diode

The current-voltage ( $I$ - $V$ ) and power-current ( $P$ - $I$ ) responses of a Ag/180-min-annealed  $\text{SiO}_2:\text{Si}^+/\text{n}$ -type Si substrate/Al (referred to as Ag/ $\text{SiO}_2:\text{Si}^+/\text{n}$ -Si/Al) MOS diode are shown in Fig. 8. The threshold current, voltage, and electric field of the Ag/ $\text{SiO}_2:\text{Si}^+/\text{n}$ -Si/Al MOS diode are 0.15 A/cm<sup>2</sup>, 3.3 V, and 66 kV/cm, which are almost one order of magnitude smaller than that of a Ag/ $\text{SiO}_2/\text{n}$ -Si/Al diode reported by Yuan and Haneman.<sup>35</sup> Such a low turn-on

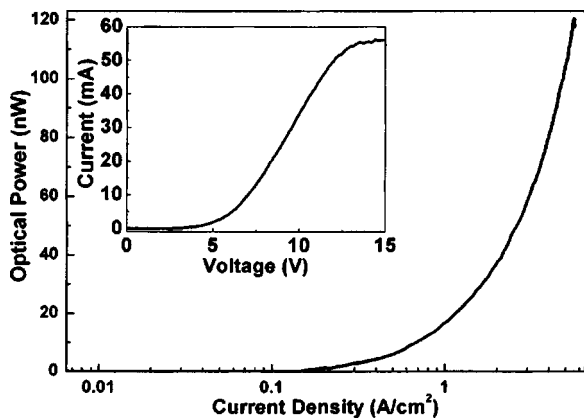


FIG. 8.  $P$ - $I$  and  $I$ - $V$  (inset) responses of EL from the Ag/ $\text{SiO}_2:\text{Si}^+/\text{n}$ -Si/Al MOS diode.

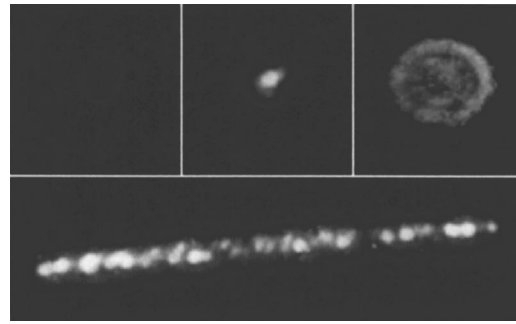


FIG. 9. Far-field EL patterns of the Ag/ $\text{SiO}_2:\text{Si}^+/\text{n}$ -Si/Al MOS diode at different bias voltages of 3.8 V (left), 12 V (middle), and 15 V (right). Lower part: the bright edge-emitting far-field pattern of the Ag/ $\text{SiO}_2:\text{Si}^+/\text{n}$ -Si/Al MOS diode at bias of 12 V.

voltage for the emission of light from the  $\text{SiO}_2:\text{Si}^+$  sample with a thickness of 500 nm is mainly attributed to the improvement (modification) of the carrier transport of the Ag/ $\text{SiO}_2:\text{Si}^+/\text{Si}/\text{Al}$  MOS diode, which is strongly related to the enhanced Fowler-Nordheim tunneling behavior of the multienergy Si implantation process. Besides, the other transparent schemes, such as hopping, also take place concurrently such that the current can be as large as several milliamperes. These results have revealed that the EL mechanism of the Si-rich  $\text{SiO}_2:\text{Si}^+$  layer may somewhat differ from that of typical semiconductors, which originates from the electron-hole recombination under forward-bias conditions.<sup>24,36,37</sup> The maximum optical output power is about 120 nW at a bias voltage of 15 V, corresponding to the bias current and electric field of 56 mA and 300 kV/cm, respectively. The resistances of the Ag/ $\text{SiO}_2:\text{Si}^+/\text{n}$ -Si/Al MOS diode before and after turn-on are 1.9 k $\Omega$  and 250  $\Omega$ , respectively.

The EL of the Ag/ $\text{SiO}_2:\text{Si}^+/\text{n}$ -Si/Al MOS diode is only observed under reverse biases with a  $P$ - $I$  slope of 2.2  $\mu\text{W}/\text{A}$  (see Fig. 9), which facilitates the injection of the minority holes accumulated in the inversion layer beneath the  $\text{SiO}_2:\text{Si}^+/\text{n}$ -Si interface. Yuan and Haneman<sup>35</sup> observed the visible EL from a negatively biased Ag/native- $\text{SiO}_2/\text{n}$ -type Si substrate/Al (referred to as Ag/ $\text{SiO}_2/\text{n}$ -Si/Al). Bae *et al.*<sup>24</sup> also reported that strong EL can only be observed in a Au/ $\text{SiO}_x/p$ -Si structure under reverse-bias conditions. A forward bias fails to induce EL since the holes can hardly be injected from the positively biased metal contact. In particular, the EL of the Ag/ $\text{SiO}_2:\text{Si}^+/\text{n}$ -Si/Al MOS diode under the reverse bias of 15 V deviates slightly from the PL of a 5000- $\text{\AA}$ -thick, 180-min-annealed  $\text{SiO}_2:\text{Si}^+$ , as compared in Fig. 10. In principle, the PL is obtained by optically pumping all of the ground-state electrons in different defects of  $\text{SiO}_2:\text{Si}^+$ , whereas the EL of the Ag/ $\text{SiO}_2:\text{Si}^+/\text{n}$ -Si/Al sample results from bias-dependent carrier injection or impact ionization of different defects in  $\text{SiO}_2:\text{Si}^+$ . The PL intensity is determined by the concentration of defects, but EL intensity is determined by the density of the minority holes in  $n$ -type Si substrate tunneling into the defect ground states. A negative bias provides energy for the electrons and holes to tunnel from the metal and the  $n$ -Si substrate into the ground and excited states of the luminescent defects in the  $\text{SiO}_2:\text{Si}^+$ . The minority-hole tunneling process is dominated

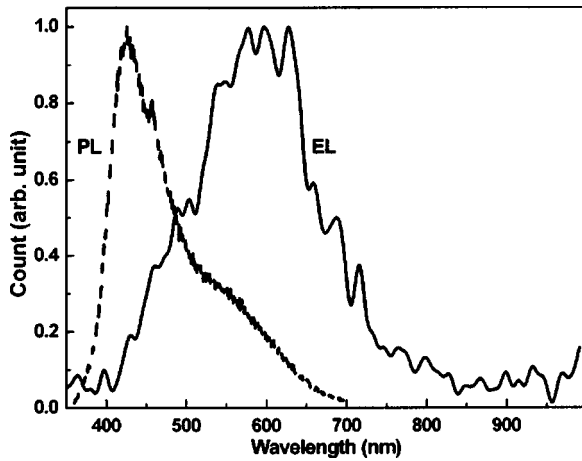


FIG. 10. Normalized PL (dashed) and EL (solid) spectra of the 180-min-annealed  $\text{SiO}_2:\text{Si}^+$  and the  $\text{Ag}/\text{SiO}_2:\text{Si}^+/\text{n-Si}/\text{Al}$  MOS diode at bias current of 15 V.

even though the impact ionization process also occurs in the  $\text{SiO}_2:\text{Si}^+$  at higher biases. Besides, a high electric field required to initiate the impact ionization process usually causes the substrate overheating effect.

A redshift phenomenon of the EL from deep blue to white and green-yellow light was observed with the increasing bias voltage or current, as shown in the upper part of Fig. 10. The change in EL color can be persuasively interpreted using the energy-band diagram of the  $\text{SiO}_2:\text{Si}^+$ . The deep-blue EL spectrum of the  $\text{Ag}/\text{SiO}_2:\text{Si}^+/\text{n-Si}/\text{Al}$  MOS diode (see the left in Fig. 9) at the bias voltage of 3.8 V is located between 350 and 450 nm. The white-light EL spectrum of the  $\text{Ag}/\text{SiO}_2:\text{Si}^+/\text{n-Si}/\text{Al}$  MOS diode at the bias voltage of 12 V (corresponding to a bias current of 50 mA) is ranging between 400 and 700 nm. Under such operation, a bright edge-emitting far-field pattern of the  $\text{Ag}/\text{SiO}_2:\text{Si}^+/\text{n-Si}/\text{Al}$  MOS diode can be observed (see lower part in Fig. 9). As the bias voltage exceeds 13 V, the intensity of output power tends to saturate and the green luminescence is clearly enhanced. It is worth noting that the EL centers of the  $\text{Ag}/\text{SiO}_2:\text{Si}^+/\text{n-Si}/\text{Al}$  MOS diode are changed under different bias. Under a reverse bias, an inversion layer can be formed beneath the  $\text{SiO}_2:\text{Si}^+/\text{n-Si}$  interface, which accumulates the minority carriers (holes) in  $\text{n-Si}$ . As the inversion layer becomes more bending at higher biases, the accumulated minority holes can be gradually tunneling into the ground states of weak-oxygen bond defect, NOV defects, and  $E'_\delta$  defects in the  $\text{Ag}/\text{SiO}_2:\text{Si}^+/\text{n-Si}/\text{Al}$  MOS diode. A stronger bias seriously bends the inversion layer beneath the  $\text{SiO}_2:\text{Si}^+/\text{n-Si}$  interface and thus greatly accumulates the holes at lower states, which facilitates the tunneling of the minority holes into the ground states of defects with smaller band-to-band transition energy, such that the transitions contributed to the luminescence at longer wavelengths can be greatly enhanced. The green EL contributed by  $E'_\delta$  defects thus becomes dominated when the bias current becomes extremely high.

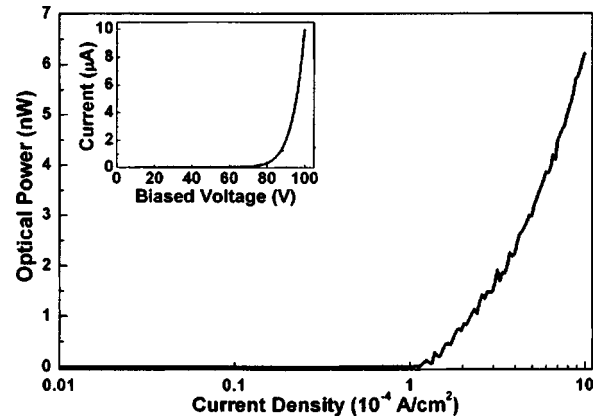


FIG. 11.  $P$ - $I$  and  $I$ - $V$  (inset) responses of the  $\text{ITO}/\text{Si-rich SiO}_x/\text{p-Si}/\text{Al}$  MOS diode.

### B. EL and $I$ - $V$ of PECVD-grown $\text{SiO}_x$ -based MOS diode

The  $I$ - $V$  and  $P$ - $I$  responses of the MOS diode made on 30-min-annealed PECVD-grown Si-rich  $\text{SiO}_x$  are shown in Fig. 11. The forward turn-on voltage and current density are 86 V and  $215 \mu\text{A}/\text{cm}^2$ , respectively. The maximum output power of 7 nW associated with a  $P$ - $I$  slope of 0.7 mW/A is determined. In contrast with the  $\text{SiO}_2:\text{Si}^+$ -based one, the  $\text{ITO}/\text{Si-rich SiO}_x/\text{Si}/\text{Al}$  MOS diode exhibits similar EL responses under both forward and reverse biases. However, higher reverse-bias condition is required to form an inverse  $n$ -channel at  $\text{SiO}_x/\text{p-Si}$  interface. The tunneling-based carrier transport mechanism is dominated due to the exponential-like  $I$ - $V$  behavior. The PECVD-grown Si-rich  $\text{SiO}_x$  sample shows a higher turn-on voltage as compared to the  $\text{SiO}_2:\text{Si}^+$  sample, which is attributed to the fewer nonradiated and irradiated defects within the PECVD-grown Si-rich  $\text{SiO}_x$  material. A better crystallinity of the PECVD-grown  $\text{SiO}_x$  film makes the current hard to tunnel through, which has also been corroborated by the lack of structural damage (WOB and NOV defects) -related PL and EL signals at blue-green region. The far-field pattern of the  $\text{ITO}/\text{Si-rich SiO}_x/\text{Si}/\text{Al}$  MOS diode at a forward bias of 100 V is shown in Fig. 12. The EL spectrum of 30-min-annealed PECVD-grown Si-rich

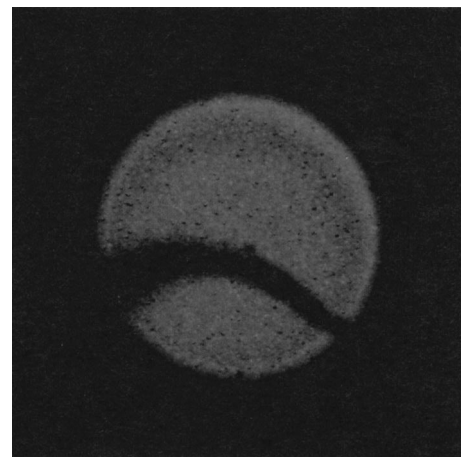


FIG. 12. Far-field EL pattern of the  $\text{ITO}/\text{Si-rich SiO}_x/\text{p-Si}/\text{Al}$  MOS diode biased at 100 V.

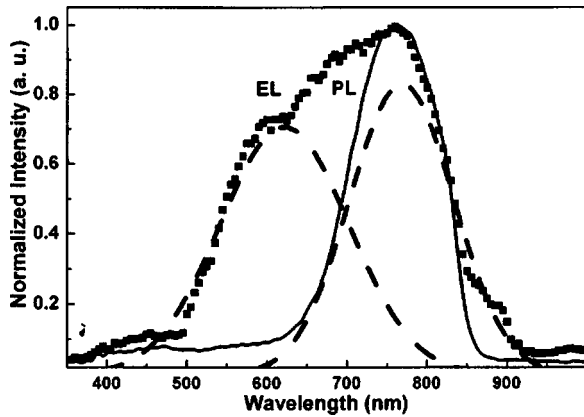


FIG. 13. Normalized PL (solid) and EL (square dotted) spectra of the 30-min-annealed PECVD-grown Si-rich  $\text{SiO}_x$  and the ITO/Si-rich  $\text{SiO}_x/p$ -Si/Al MOS diode biased at 100 V. The decomposed EL components at 625 and 768 nm are shown (dashed).

$\text{SiO}_x$ -based ITO/Si-rich  $\text{SiO}_x/\text{Si}/\text{Al}$  MOS diode sample is shown in Fig. 13, which is decomposed into dual luminescent peaks at wavelengths of 625 and 768 nm with spectral linewidths of 189 and 154 nm, respectively. Note that the EL components at longer wavelength coincide well with that of PL, which reveals that the nc-Si-related PL and EL are attributed to the same carrier recombination mechanism in the buried nc-Si. Franzo *et al.*<sup>20</sup> have attributed the EL at 700–850 nm to the impact ionization and recombination in buried nc-Si. More important, Irrera *et al.*<sup>38</sup> clarified that the impact ionized carriers are confined and recombined within the nc-Si without accelerating under the high electric field. De La Torre *et al.*<sup>39</sup> found a very weak temperature dependence on the  $I$ - $V$  response of the Al/ $\text{SiO}_x$ :nc-Si/ $p^+$ -Si light-emitting diode (LED) with a 40-nm-thick  $\text{SiO}_2$  film, which is relatively in agreement with the tunneling conduction process. Our results indicate that the Fowler–Nordheim (FN) process did not occur due to a low electric field of  $<5$  MV/cm. It is thus concluded that the carriers in nc-Si are neither thermally activated nor field-enhanced FN tunneling injected, but is possibly assisted by direct tunneling between nc-Sis.<sup>38</sup>

However, the mechanism of secondary EL peak expanded to shorter-wavelength region (500–700 nm) is yet unclear. Previously, Franzo *et al.*<sup>20</sup> suggested that the blueshifting EL is mainly due to the impact excitation of smaller nc-Si (emitting at shorter wavelength) by the injected carriers with increasing energies under high biased condition. Even though, the effect of oxygen-related defects on the secondary EL at about 660 nm was ever considered. De La Torre *et al.*<sup>39</sup> also attributed the 540–690-nm EL to the pre-existing defects in the  $\text{SiO}_2$  matrix. Similar EL side peak at 650 nm was discovered by Valenta *et al.*<sup>17</sup> Up to now, no further explanations are addressed on the enhancement of short-wavelength EL under electrical instead of optical pumping process. Nonetheless, a possible cold-carrier tunneling process was considered to happen in the ITO/Si-rich  $\text{SiO}_x/\text{Si}/\text{Al}$  MOS diode under appropriate bias.<sup>40</sup> Since the band structure of Si-rich  $\text{SiO}_x$  is seriously bending under extremely high electric field, the electrons could tunnel from a first-order quantized state ( $n=1$ ) in one nc-Si to a second-

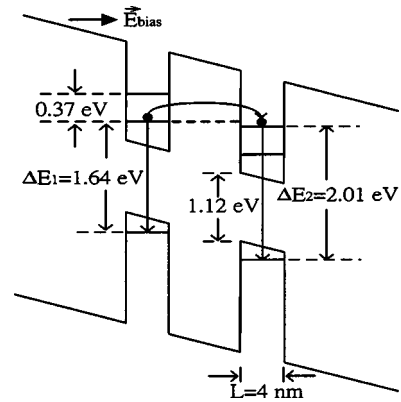


FIG. 14. The cold-carrier tunneling mechanism happened in high-excited states between adjacent nc-Si quantum dots in the ITO/Si-rich  $\text{SiO}_x/p$ -Si/Al MOS structure.

order quantized state ( $n=2$ ) in the adjacent nc-Si, as illustrated in Fig. 14. This provides a higher population in the second-order ( $n=2$ ) state as well as an enhanced spontaneous emission at larger energy. According to the theory of quantum combined systems,<sup>40,41</sup> the band-to-band transition energies of first-order and second-order excited states for a nc-Si quantum dot with the diameter of 4 nm are calculated as  $\Delta E_1=1.64$  eV (or  $\lambda_1=756$  nm) and  $\Delta E_2=2.01$  eV (or  $\lambda_2=616$  nm), respectively. These values exactly coincide with the wavelength of the EL components decomposed from our experimental results, the energy difference between two transitions is theoretically calculated as  $\Delta E_{l=2 \rightarrow l=1} = 3\pi^2\hbar^2/2m_e^*L^2 = 0.37 \pm 0.01$  eV, where  $l$ ,  $m_e^*$ , and  $L$  denote the angular momentum state, the electron effective mass, and the diameter of nc-Si quantum dot, respectively.<sup>41</sup> In contrast, there is no significant PL contributed by the second-order states as compared to that contributed by the first-order states in view of the previous reports, which could be attributed to the absence of band-filling effect under such a low pumping density in PL measurements. The second-order state-related PL is detectable as the first-order states are fulfilled by increasing the pumping flux density of photons. These observations primarily elucidate that the bias-dependent and blueshifted EL is mainly attributed to the cold-carrier tunneling induced high-excited state transition effect between adjacent nc-Si quantum dots under a sufficiently high electric field.

## V. CONCLUSIONS

Oxygen defect-dependent white-light electroluminescence from a  $\text{SiO}_2:\text{Si}^+$  MOS diode, and Si nanocrystal-dependent near-infrared electroluminescence from a PECVD-grown Si-rich  $\text{SiO}_2$  MOS diode have been investigated. The Si-ion implantation introduces enormous radiative defects into the  $\text{SiO}_2$  film, which causes a strong PL peak at around 410–460 nm after annealing the  $\text{SiO}_2:\text{Si}^+$  at 1100 °C for 180 min. Three radiative defects in the  $\text{SiO}_2:\text{Si}^+$  sample, including WOB, NOV, and  $E'\delta$  defects corresponding to PL at 415, 455, and 520 nm, respectively, are confirmed by  $C$ - $V$  and EPR measurements. The generation of NOV and WOB is described by the reaction of  $\text{O}_3 \equiv \text{Si}-\text{O}-\text{Si} \equiv \text{O}_3 \rightarrow \text{O}_3 \equiv \text{Si}-\text{Si} \equiv \text{O}_3 + \text{O}_{\text{interstitial}}$  and  $\text{O}_{\text{interstitial}} + \text{O}_{\text{interstitial}} \rightarrow \text{O}-\text{O}$ .

The white-light EL of the Ag/SiO<sub>2</sub>:Si<sup>+</sup>/n-Si/Al MOS diode is only observed under reverse biases with a  $P$ - $I$  slope of 2.2  $\mu$ W/A, due to the injection of the minority holes accumulated in the inversion layer beneath the SiO<sub>2</sub>:Si<sup>+</sup>/n-Si interface. The threshold current (voltage) and the maximum optical output power of 0.15 A/cm<sup>2</sup> (3.3 V) and 120 nW, respectively, are reported. The PL is obtained by optically pumping all of the ground-state electrons in different defects of SiO<sub>2</sub>:Si<sup>+</sup>, whereas the EL of the Ag/SiO<sub>2</sub>:Si<sup>+</sup>/n-Si/Al sample results from bias-dependent carrier injection or impact ionization of different defects in SiO<sub>2</sub>:Si<sup>+</sup>, providing different emission colors with increasing biases. For the PECVD-grown Si-rich SiO<sub>x</sub> annealed at 1100 °C for 30 min, the peak PL at 760 nm attributed to the nc-Si is observed and a supporting evidence of the nc-Si with diameters of 4–5 nm is given by the HRTEM analysis. Longer annealing time induced reoxidation effect of nc-Si inevitably makes the PL broadened and blueshifted. However, the ITO/Si-rich SiO<sub>x</sub>/Si/Al MOS diode exhibits a smaller output power of 7 nW with an extremely high turn-on voltage of 86 V, which is due to the less pronounced effect of carriers tunneling through such a better crystalline PEVCD-grown SiO<sub>x</sub>. In comparison, the EL at longer wavelength coincides well with that of PL, which reveals that the nc-Si-related PL and EL are attributed to the same carrier recombination mechanism in the buried nc-Si. The EL of the ITO/Si-rich SiO<sub>x</sub>/Si/Al MOS diode is mainly due to the transfer of cold carriers by direct tunneling between adjacent nc-Sis. The cold-carrier tunneling process from lower-excited state to higher-excited state between two adjacent nc-Si quantum dots under high electric field is primarily elucidated. The difference between the PL and EL results is also explained with the proposed mechanism.

## ACKNOWLEDGMENT

This work was supported in part by the National Science Council (NSC) of the Republic of China under Grant Nos. NSC93-2215-E-009-007 and NSC92-2215-E-009-028.

<sup>1</sup>Q. Ye, R. Tsu, and E. H. Nicollian, *Phys. Rev. B* **44**, 1806 (1991).

<sup>2</sup>A. Pèrez-Rodríguez, O. González-Varona, B. Garrido, P. Pellegrino, J. R. Morante, C. Bonafos, M. Carrada, and A. Claverie, *J. Appl. Phys.* **94**, 254 (2003).

<sup>3</sup>D. Pacifici, E. C. Moreira, G. Franzo, V. Martorino, and F. Priolo, *Phys. Rev. B* **65**, 144109 (2002).

<sup>4</sup>L. T. Canham, *Appl. Phys. Lett.* **57**, 1046 (1990).

<sup>5</sup>X. Zhao, O. Schoenfeld, J. Kusano, Y. Aoyagi, and T. Sugano, *Jpn. J. Appl. Phys., Part 2* **33**, L899 (1994).

<sup>6</sup>P. Mutti, G. Ghislotti, S. Bertoni, L. Bonoldi, G. F. Cerofolini, L. Meda, E. Grilli, and M. Guzzi, *Appl. Phys. Lett.* **66**, 851 (1995).

<sup>7</sup>T. Shimizu-Iwayama, K. Fujita, S. Nakao, K. Saitoh, T. Fujita, and N. Itoh, *J. Appl. Phys.* **75**, 7779 (1994).

<sup>8</sup>H. Takagi, H. Owada, Y. Yamazaki, A. Ishizaki, and T. Nakagiri, *Appl. Phys. Lett.* **56**, 2379 (1990).

<sup>9</sup>S. Tong, X. N. Liu, T. Gao, and X. M. Bao, *Appl. Phys. Lett.* **71**, 698 (1997).

<sup>10</sup>L. S. Liao, X. M. Bao, X. Q. Zheng, N. S. Li, and N. B. Min, *Appl. Phys. Lett.* **68**, 850 (1996).

<sup>11</sup>H. Z. Song, X. M. Bao, N. S. Li, and J. Y. Zhang, *J. Appl. Phys.* **82**, 4028 (1997).

<sup>12</sup>G. G. Qin, A. P. Li, B. R. Zhang, and B. C. Li, *J. Appl. Phys.* **78**, 2006 (1995).

<sup>13</sup>H. Z. Song and X. M. Bao, *Phys. Rev. B* **55**, 6988 (1997).

<sup>14</sup>W. Hayes, M. J. Kane, O. Salminen, R. L. Wood, and S. P. Doherty, *J. Phys. C* **17**, 2943 (1984).

<sup>15</sup>H. Nishikawa, E. Watanabe, D. Ito, M. Takiyama, A. Leki, and Y. Ohki, *J. Appl. Phys.* **78**, 842 (1995).

<sup>16</sup>R. Tohmon, Y. Shimogaichi, H. Mizuno, Y. Ohki, K. Nagasawa, and Y. Hama, *Phys. Rev. Lett.* **62**, 1388 (1989).

<sup>17</sup>J. Valenta, N. Lalic, and J. Linnros, *Opt. Mater. (Amsterdam, Neth.)* **17**, 45 (2001).

<sup>18</sup>J. Valenta, R. Juhasz, and J. Linnros, *Appl. Phys. Lett.* **80**, 1070 (2002).

<sup>19</sup>F. Iacona, F. Frazo, E. C. Moreira, D. Pacifici, A. Irrera, and F. Priolo, *Mater. Sci. Eng., C* **19**, 377 (2002).

<sup>20</sup>G. Franzo *et al.*, *Appl. Phys. A: Mater. Sci. Process.* **74**, 1 (2002).

<sup>21</sup>L. Skuja, *J. Non-Cryst. Solids* **149**, 77 (1992).

<sup>22</sup>J. C. Cheang-Wong, A. Oliver, J. Roiz, J. M. Hernandez, L. Rodrigues-Fernandez, J. G. Morales, and A. Crespo-Sosa, *Nucl. Instrum. Methods Phys. Res. B* **175–177**, 490 (2001).

<sup>23</sup>H. Nishikawa, R. E. Stahlbush, and J. H. Stathis, *Phys. Rev. B* **60**, 15910 (1999).

<sup>24</sup>H. S. Bae, T. G. Kim, C. N. Whang, S. Im, J. S. Yun, and J. H. Song, *J. Appl. Phys.* **91**, 4078 (2002).

<sup>25</sup>E. H. Poindexter and P. J. Caplan, *J. Vac. Sci. Technol. A* **6**, 1352 (1988).

<sup>26</sup>B. L. Zhang and K. Raghavachari, *Phys. Rev. B* **55**, R15993 (1997).

<sup>27</sup>H. Nishikawa, R. Nakamura, R. Tohmon, Y. Ohki, Y. Sakurai, K. Nagasawa, and Y. Hama, *Phys. Rev. B* **41**, 7828 (1990).

<sup>28</sup>S. T. Chou, J. H. Tsai, and B. C. Sheu, *J. Appl. Phys.* **83**, 5394 (1998).

<sup>29</sup>H. Nishikawa, E. Watanabe, D. Ito, Y. Sakurai, K. Nagasawa, and Y. Ohki, *J. Appl. Phys.* **80**, 3513 (1996).

<sup>30</sup>M. Ya. Valakh, V. A. Yukhimchuk, V. Ya. Bratus, A. A. Konchits, P. L. F. Hemment, and T. Komoda, *J. Appl. Phys.* **85**, 168 (1999).

<sup>31</sup>K. Vanheusden and A. Stesmans, *J. Appl. Phys.* **74**, 275 (1993).

<sup>32</sup>Y. Sakurai and K. Nagasawa, *J. Appl. Phys.* **86**, 1377 (1999).

<sup>33</sup>H. Nishikawa, T. Shiroyama, R. Nakamura, Y. Ohki, K. Nagasawa, and Y. Hama, *Phys. Rev. B* **45**, 586 (1992).

<sup>34</sup>C. Delerue, G. Allan, and M. Lannoo, *Phys. Rev. B* **48**, 11024 (1993).

<sup>35</sup>J. Yuan and D. Haneman, *J. Appl. Phys.* **86**, 2358 (1999).

<sup>36</sup>M. Kimura and H. Koyama, *J. Appl. Phys.* **85**, 7671 (1999).

<sup>37</sup>H. J. Wen and R. Ludeke, *J. Vac. Sci. Technol. B* **15**, 1080 (1997).

<sup>38</sup>A. Irrera *et al.*, *Appl. Phys. Lett.* **81**, 1866 (2002).

<sup>39</sup>J. De La Torre *et al.*, *Physica E (Amsterdam)* **16**, 326 (2003).

<sup>40</sup>D. J. DiMaria *et al.*, *J. Appl. Phys.* **56**, 401 (1984).

<sup>41</sup>D. K. Ferry and S. M. Goodnick, in *Transport in Nanostructures* (Cambridge University Press, New York, 1997), pp. 23–90.